**HEFAT2014**
**10th International Conference on Heat Transfer, Fluid Mechanics and Thermodynamics**
**14 – 16 July 2014**
**Orlando, Florida**

# HEAT TRANSFER WITH PHASE CHANGE IN A SHELL AND TUBE LATENT HEAT STORAGE UNIT

García-Alonso J. M., Aguilar F. and Montero E.*
*Author for correspondence
Department of Electromechanical Engineering, Escuela Politécnica Superior
University of Burgos,
Burgos, 09006,
Spain,
E-mail: emontero@ubu.es

## ABSTRACT

Concerning thermal energy storage, latent heat thermal energy storage is particularly attractive technique because it provides a high energy storage density. The development of a latent heat thermal energy storage system therefore involves first the understanding of heat transfer in the phase change materials (PCM) when they undergo solid-to-liquid phase transition in the required operating temperature range, and second, the design of the container for holding the PCM and the formulation of the phase change problem.

The paper presents a study on the heat transfer mode of a PCM stored in a horizontal cylindrical shell and tube heat exchanger, being the PCM placed inside the tubes. For this purpose, an experimental bench has been developed to test the heat transfer process, coupled with a Ground-Source Heat Pump (GSHP), controlled by a computer program developed to manage the coupled GSHP+PCM system. The aim is to compute the heat transfer of the installation during the loading, storage and downloading energy processes. More precisely, the interest is to check experimentally to what extent some common hypothesis used for heat transfer calculations are valid or not. In particular: (i) Comparison between the radial and the axial heat transfer through the wall of the PCM tube; (ii) The temperature distribution of the heat transfer fluid in the central and peripheral locations; (iii) The heat transfer rate between the container and the ambient temperature. Results indicate that density gradients could occur during energy exchange between the heat transfer fluid and the PCM when melting or solidification are taking place, leading to modification of central flow with respect to peripheral flow. Also, the temperature gradients recorded in the axial direction during the change of phase were very small compared with those of that of the radial direction, indicating essentially a two-dimensional heat transfer mode.

## INTRODUCTION

One of the present issues to improve energy efficiency is the need to store excess energy that would otherwise be wasted and also to bridge the gap between energy generation and consumption. Latent heat thermal energy storage is particularly attractive technique because it provides a high energy storage density. When compared to a conventional sensible heat energy storage system, latent heat energy storage system requires a smaller weight and volume of material for a given amount of energy. In addition, latent heat storage has the capacity to store heat of fusion at a constant or near constant temperature which corresponds to the phase transition temperature of the phase change material (PCM). Reference [1] presents a general review of thermal energy storage systems, including PCMs, while reference [2] presents a review on the PCM materials used.

Once the PCM has been selected, based primarily on the temperature range of application, the next most important factors to consider are: (i) the geometry of the PCM container and (ii) the thermal and geometrical parameters of the container required for a given amount of PCM. These factors have a direct influence on the heat transfer characteristics in the PCM and ultimately affect the melt time and the performance of the PCM storage unit.

PCMs are mostly placed in cylindrical or rectangular containers. A survey of previously published papers dealing with latent heat thermal energy storage systems shows that the most intensely analyzed unit is the shell and tube system, accounting for more than 70% [3]. This is probably due to the fact that most engineering systems use cylindrical pipes and also because heat loss from the shell and tube system is minimal.

Fig. 1 shows the classification of common PCM containers in terms of the geometry.

Three modes of cylindrical PCM container configurations are distinguished. The first is where the PCM fills the shell and the heat transfer fluid flows through a single tube, designated as the pipe model. In the second model the PCM fills the tube and the heat transfer fluid (HTF) flows parallel to the tube, said the cylinder model. The third cylinder model is the shell and tube system. Several authors [4-6] recommend shell and tube configuration as it performs heat transfer better than the pipe model.

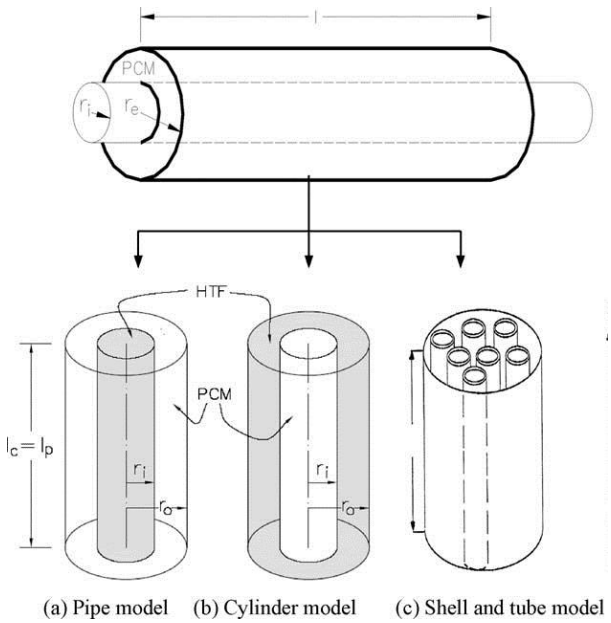


**Figure 1.** Classification of common PCM containers in terms of the geometry.

In a cylindrical container there exist two possibilities for the flow direction of the heat transfer fluid during charging and discharging of the PCM energy. The two modes are the parallel flow (either the hot and cold fluids are introduced into the heat exchanger from the same end) and the counter-current flow (the hot and cold fluids are introduced from the opposite ends). Fig. 2 illustrates the schematic diagram of the parallel and counter-current flow principles.

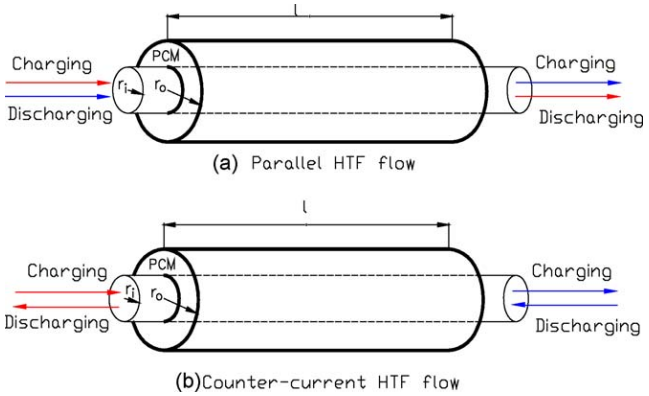


**Figure 2**. The physical model of parallel and counter-current HTF flow in a shell and tube heat exchanger.

For each pair, the upper arrow represents the direction of HTF flow during charging and the lower arrow represents discharge direction of the HTF.

Gong and Mujumdar [7] investigated the effect of the parallel and counter-current flow modes and showed that parallel flow increases the energy charge/discharge rate by 5% more than counter-current flow.

Apart from the container geometry and configuration, some other thermal and geometric parameters are known to affect the thermal performance of latent heat thermal energy storage systems. For example, shell and tube containers often place baffles to support the tubes, and then parallel, counter-current and angular flows could take place inside the cylinder container. Then, tests and experimental data should be performed to test mathematical modelling and simulation of heat transfer modes.

This paper presents a study on the heat transfer mode of a PCM stored in a horizontal cylindrical shell and tube heat exchanger, being the PCM placed inside the tubes. For this purpose, an experimental bench has been developed to test the heat transfer process, coupled with a Ground-Source Heat Pump (GSHP), controlled by a computer program developed to manage the coupled GSHP+PCM system. The aim is to compute the heat transfer of the installation during the loading, storage and downloading energy processes. More precisely, the interest is to check experimentally to what extent some common hypothesis used for heat transfer calculations are valid or not. In particular: (i) Comparison between the radial and the axial heat transfer through the wall of the PCM tube; (ii) The temperature distribution of the heat transfer fluid in the central and peripheral locations; (iii) The heat transfer rate between the container and the ambient temperature.

## NOMENCLATURE

| | | |
|---|---|---|
| $A$ | [$m^2$] | Area |
| $AD$ | [ºC] | Average difference of temperature |
| $e$ | [m] | Thickness |
| $E$ | [J] | Energy |
| $k$ | [W/mK] | Thermal conductivity |
| $MRD$ | [%] | Maximum relative difference |
| $Q$ | [W] | Power (heat) |
| $r$ | [m] | Radius |
| $R_{th}$ | [K/W] | Thermal resistance |
| $RAD$ | [%] | Relative average difference |
| $t$ | [s] | time |
| $T$ | [ºC] | Temperature |

Special characters

| | | |
|---|---|---|
| $\Delta$ | [-] | Difference |

## EXPERIMENTAL APPARATUS

To test the heat transfer mode of a horizontal cylindrical shell and tube container for PCM energy storage, an experimental bench has been designed and built, as shown in Fig. 3.

The PCM used is a hydrated salt with a melting temperature of 41ºC. It was selected because it is an adequate temperature for domestic hot water production and radiant floor heating. Table 1 presents the thermo-physical properties of the PCM, obtained from reference [8].

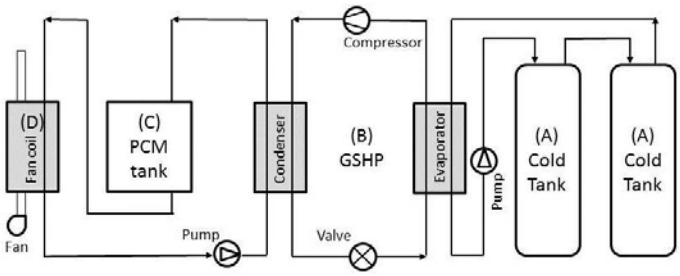


**Figure 3**. Diagram of the experimental bench for testing the heat transfer rate of PCM placed in a cylindrical shell and tube container.

The PCM used is a hydrated salt with a melting temperature of 41ºC. It was selected because it is an adequate temperature for domestic hot water production and radiant floor heating. Table 1 presents the thermo-physical properties of the PCM, obtained from reference [8].

The storage temperature and the size of the container has been chosen to meet the energy needs for the heating and the domestic hot water supply of a single family house of about 150 $m^2$. A Ground-Source Heat Pump (GSHP) supply the energy needed to charge/discharge the PCM energy storage.

**Table 1**. Thermo-physical properties of the PCM placed inside the cylindrical container [8].

| Phase Change Temperature (ºC) | | Latent Heat Capacity (kJ/kg) | | Density ($kg/m^3$) |
|---|---|---|---|---|
| 41 | | 210 | | 1587 |
| Specific Heat Capacity (kJ/kg·K) | | Thermal Conductivity (W/m·K) | | |
| Solid | Liquid | Solid | Liquid | |
| 1,68 | 2,59 | 0.450 | 0.245 | |

The experimental bench consists of (A) two water tanks, from Domusa™, model SANIT 150, each one of 150 l of volume, equipped with temperature control to set the temperature of the cold-source of the heat pump between 10ºC and 40ºC; (B) the GSHP from Giordano™, model SUNEO N5 (open loop heat pump, which uses the two tanks A as if they were aquifer energy sources), nominal heating power 5.35 kW, fluid R-407C; (C) one horizontal storage tank of 210 l, filled with the PCM modules; (D) one fan-coil Saunier Duval™, model 3-020 AF, to dissipate the energy stored in the PCM water tank, simulating the energy use in a single family house. For energy calculation purposes, the experimental stand was equipped with thermal energy meters Kundo™, model G20/G21, class B, which includes two temperature probes Pt1000 and a flow meter with a maximum relative error of ±4%. All the measurement devices are computer controlled by means of the Agilent VEE 7.0 software.

The PCM is encapsulated in cylindrical tubes, each of 1000 mm long and 50 mm external diameter, 2 mm thickness. The tubes are made of high density polyethylene, with a thermal conductivity of 0.2 W/m·K.

The stainless steel cylindrical tank is 1020 mm long and 510 mm internal diameter, with a capacity of 210 l. It is placed in horizontal position, with 1" diameter of input and output nozzles. The tank is externally insulated with a blanket of thickness 50 mm made of a commercial elastomer whose thermal conductivity is 0.04 W/m·K.

Five baffles are placed inside the container, to stand the PCM tubes in horizontal position, then the container could be considered as a shell and tube one. A maximum of 24 PCM tubes can be allocated inside the container. The holes of the baffles are made of higher diameter than those of the PCM tubes, in order to allow the water-flow. Fig. 4 shows the geometrical distribution of PCM tubes.


**Figure 4**. Configuration of PCM tubes and baffles inside the circular section of the container.

A set of 10 Pt100 temperature probes have been used to obtain the temperature distribution inside the shell and tube tank, as shown in Fig. 5. T103 to T107 probes measure the outside temperature of the tank, T102 measures the inner water temperature, T115 and T116 register the temperature of the internal surface of the PCM tubes and T117 and T118 measure the temperature of the external surface of the same. Ambient temperature, and inlet and outlet temperatures of water are also measured.

Temperature measurement was performed by means of the Pt100 probes and the multi-meter Agilent 34970A. After calibration of the equipment, uncertainty of temperature measurement has been estimated to be less than 0.05 K.

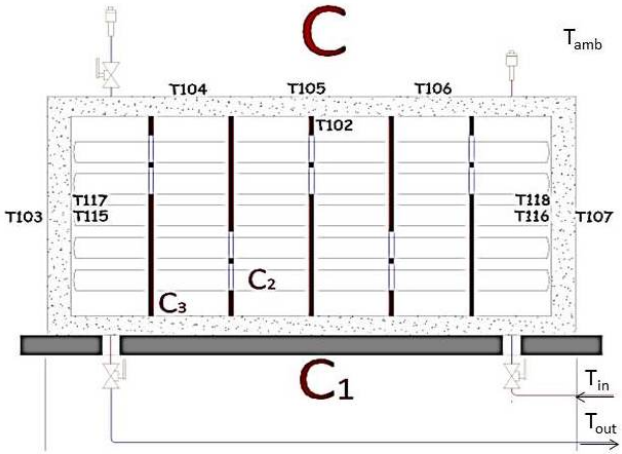


**Figure 5**. Distribution of Pt100 temperature probes in the shell and tube cylindrical container C. PCMs are placed inside the tubes ($C_2$) while water flows by the external surface ($C_3$).

Fig. 6 shows a typical energy charging/discharging mode of the PCM storage tank on a daily basis. The conditions during the experiment are that GSHP operates 14 h (from 22.00h to 12.00h, when the electricity cost is cheaper) while the fan-coil operates 24.00h (all day house demand). The hot water as HTF is supplied by the GSHP, and the set point is fixed at 50ºC. During the charging period, the GSHP starts heating the HTF, and the PCM in solid phase increases its temperature during the sensible heat transfer stage, before melting, showing a quasi-linear slope in the increasing temperature. When the melting temperature of PCM is reached (41ºC) at the external surface of the PCM, it starts changing to the latent heat transfer mode and melting process takes place. The rate of temperature increase is smaller, and the slope of the curve then decreases compared to the sensible mode. Along this period, heat from the HTF is transferred to the PCM through the thermal resistance of the polyethylene tube by heat conduction. The external annulus of the PCM is in the liquid phase, while the internal circular section is still solid, as shown in Fig. 7.

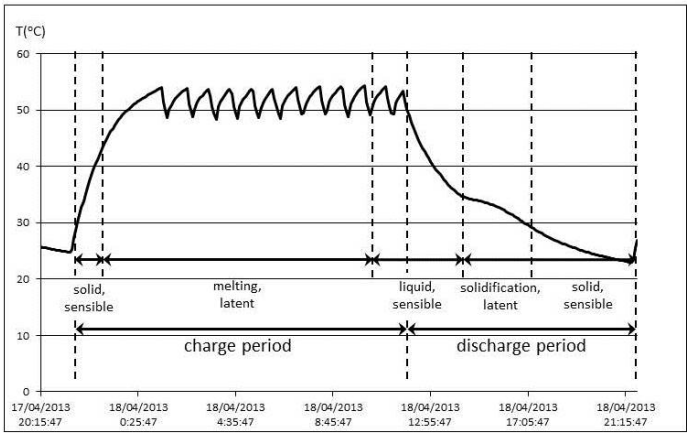


**Figure 6**. Distribution of the storage tank temperature vs. time during the charge and discharge periods of the PCM container.

The PCM liquid phase transfers sensible heat between the temperature $T_2$ and the liquid-solid boundary temperature $T_m$, which is the melting temperature. The solid phase is expected to be at $T_m$, and new energy transfer produces melting and the boundary moves to an inner radio. The heat balance across the interface, known as Stefan condition [9], means that the latent heat released due to the interface displacement equals the net amount of heat delivered to (or from) the interface per unit area and unit time (flux normal to the moving surface).

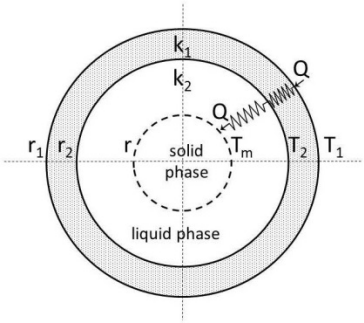


**Figure 7**. Heat transfer during the melting process. $T_1$ = external temperature of the polyethylene tube at $r_1$; $T_2$ = internal temperature of the polyethylene tube and external temperature of the PCM liquid phase at $r_2$; $T_m$ = boundary melting temperature at the moving boundary $r$.

Once the set-point of 50ºC is reached by the HTF, typical temperature evolution of the temperature in a saw-tooth shape around the temperature set point occurs, as the GSHP is on/off controlled. This mode is kept repeatedly along the rest of the charging period. Along this period, the PCM ends its melting and all the PCM is in the liquid phase. Moreover, superheating of the liquid PCM should take place if the GSHP still continues working. It should be noticed that, at a fixed time, the radius of the moving boundary of the melting PCM will be different along the axial direction of the tube, and also the temperature of the liquid phase in contact with the local temperature of the HTF.

When the GSHP ends its heat supply, only the fan-coil is in operation, and the discharging period starts, the PCM being in the liquid phase. Initially, the PCM temperature decreases as sensible heat exchanges, and super-cooling of the PCM (under its nominal solidification temperature) could sometimes appear. When solidification of the PCM begins, the temperature profile shows a nearly flat shape, enlarging the period of time of energy availability at a useful temperature, which constitutes one of the advantages of the PCM. After the solidification ends, then the discharge uses the sensible heat exchange of the solid PCM.

## RESULTS AND DISCUSSION

Several tests were conducted to study the heat transfer phenomena in the cylindrical container. The temperature control of the two water tanks (A), acting as low temperature heat reservoirs, was set to 20ºC. The temperature of the water supply by the GSHP was set to 50ºC, equipped with an off/on control regulated by the return line of HTF. The charging cycle

of the GSHP was programmed to operate along 14 h, from 22.00h to 12.00h. Three discharging modes were studied, using three air flow rates at the fan-coil (D), 160 $m^3$/h, 250 $m^3$/h and 390 $m^3$/h, named Test 1, Test 2 and Test 3 respectively. The fan-coil was switched-on along 24 h, and then the discharging cycle duration was 10 h, from 12.00h to 22.00h. Temperature and other measurements were registered every 300 seconds, which means 288 records in a 24 h cycle.

Some energy transfer processes were studied through the three tests carried on. The interest is to check experimentally to what extent some common hypothesis used for heat transfer calculations are valid or not. In particular:

a) Comparison between the radial and the axial heat transfer through the wall of the PCM tube, made of high density polyethylene (HDPE).
b) The temperature distribution of the HTF (water) in the central and peripheral locations.
c) The heat transfer rate between the container and the ambient temperature

**Comparison between the radial and the axial heat transfer through the wall of the PCM tube.**

As stated previously, PCM is encapsulated in cylindrical tubes, each of 1000 mm long and 50 mm external diameter, 2 mm thickness. The tubes are made of HDPE, with a thermal conductivity of 0.2 W/m·K (similar to the liquid PCM and slightly smaller than that of the solid PCM). The thermal resistance $R_{th}$ is defined as

$$R_{th} = {}^{e}/_{k \cdot A} \quad (1)$$

where $e$ is the thickness of the material, $k$ the thermal conductivity and $A$ is the front area of the heat flux. In this case, as the external area of the cylinder is 0.16 $m^2$, this leads to a thermal resistance of 0.063 $K \cdot W^{-1}$, which can be similar to some other encapsulating materials.

Moreover, the temperature differences measured at both sides of tube wall are small, as shown in Table 2. At the left side of the container, near the HTF outlet, the temperatures are measured by probes T115 and T117. At the right side of the container, near the HTF inlet, the temperatures are measured by probes T116 and T118.

**Table 2**. Differences of internal/external temperatures of the PCM tubes. Average and maximum values.

| Parameter | $\Delta T_{115\text{-}117}$ | $\Delta T_{116\text{-}118}$ | Test |
|---|---|---|---|
| Relative Average Difference (%) $RAD = \frac{100}{N}\sum_{i=1}^{N}\left\|\frac{\Delta T}{T}\right\|$ | 0.730 | 0.426 | 1 |
| | 0.650 | 0.370 | 2 |
| | 0.695 | 0.424 | 3 |
| Maximum Relative Difference (%) $MRD = Max\left(100\left\|\frac{\Delta T}{T}\right\|\right)$ | 4.688 | 3.322 | 1 |
| | 3.033 | 2.641 | 2 |
| | 3.280 | 2.887 | 3 |
| Average Difference (ºC) $AD = \frac{100}{N}\sum_{i=1}^{N}\lvert\Delta T\rvert$ | 0.314 | 0.190 | 1 |
| | 0.267 | 0.162 | 2 |
| | 0.288 | 0.187 | 3 |

Average differences of temperature through the thickness of HDPE are less than 0.32ºC in any test, or less than 0.73 % in relative terms. Maximum differences between inner/outer temperatures of PCM tube occur always at the beginning of the charging period, frequently during the first 20 minutes after the GSHP started increasing the HTF temperature. Even in this case, the differences are always less than 4.7 %.

The second concern is the thermal resistance along the axial direction of the tube. At the inner side of the tube the temperatures are measured by probes T115 and T116, and the outer side temperatures are measured by probes T117 and T118. Results are shown in Table 3.

**Table 3**. Differences of axial temperatures of the PCM tubes. Average and maximum values.

| Parameter | $\Delta T_{115\text{-}116}$ | $\Delta T_{117\text{-}118}$ | Test |
|---|---|---|---|
| Relative Average Difference (%) $RAD = \frac{100}{N}\sum_{i=1}^{N}\left\|\frac{\Delta T}{T}\right\|$ | 2.822 | 2.530 | 1 |
| | 2.658 | 2.243 | 2 |
| | 2.641 | 2.288 | 3 |
| Maximum Relative Difference (%) $MRD = Max\left(100\left\|\frac{\Delta T}{T}\right\|\right)$ | 11.641 | 9.488 | 1 |
| | 8.996 | 9.389 | 2 |
| | 10.334 | 9.013 | 3 |
| Average Difference (ºC) $AD = \frac{100}{N}\sum_{i=1}^{N}\lvert\Delta T\rvert$ | 1.219 | 1.105 | 1 |
| | 1.113 | 0.965 | 2 |
| | 1.129 | 0.998 | 3 |

It can be considered that the inner temperature difference $\Delta T_{115\text{-}116}$ is representative of the PCM side, while $\Delta T_{117\text{-}118}$ is closer to the HTF temperature (water side). It can be observed that average differences of temperature along the axial direction are less than 1.22ºC in any test, which means less than 2.83 % in relative terms. As the area of the front annular surface is very small, and the considered length is 1000 mm, the thermal resistance in this case is 16556 $K \cdot W^{-1}$. That means that heat transfer along the axial direction is almost negligible compared to the radial direction.

Maximum differences of temperature along the axial direction (up to 11.65 %) take place during the initial rise of temperature of the charging mode.

**The temperature distribution of the HTF (water) in the central and peripheral locations.**

Distribution of HTF temperature along the PCM cylindrical container is measured in three sections. Related to Fig. 5, probe T117 measures the temperature of HTF just onto the external surface of the outlet side; probe T118 does the same at the inlet side; and probe T102 measures the temperature of HTF in an intermediate point of the cylinder, placed in the upper side of the central baffle that supports the tubes. Probes T117 and T118 will be more influenced by the tube temperatures, while T102 will be dominated by the HTF bulk temperature. In different sections of the tank, parallel, counter-current and angular flows could take place. Results of temperature measurement during a full charging/discharging cycle are presented in Fig. 8. When the GSHP is switched-on, the storage tank presents a positive energy balance (more energy enters than exits), as well as when the GSHP is switched-off the energy balance is negative (more energy exits than enters).

For the discussion purpose of this section, only data for Test 2 air flow rate at the fan-coil (D), 250 $m^3$/h, are presented. Similar conclusions could be obtained from the analysis of Test 1 and 3.

It can be observed that the increase of temperature during the initial phase of the charging period is almost the same for the three temperature probes, showing a uniform behavior of the HTF. It must be recalled that under the melting temperature, 41ºC, the PCM is solid and exchange sensible heat with the HTF. When the HTF is over 41ºC, the solid PCM is surrounded by an annulus of liquid PCM and its temperature rises over 41ºC, depending on the exchange of sensible heat with the HTF.

Once the HTF reaches the set-point temperature of 50ºC, the temperature behaves in a saw-tooth shape, due to the on/off control of the GSHP, though with some delay of the intermediate temperature (T102) with respect to both side temperatures (T117 and T118). Temperature of the outlet side (T117) also presents a small delay compared with the inlet side (T118). Fig. 9 shows a closer description of this phenomenon.

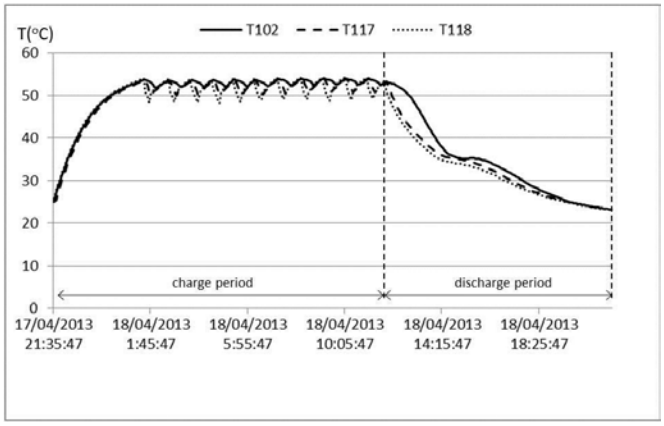


**Figure 8**. Distribution of the HTF temperature vs. time along the charge and discharge periods of the PCM container.

The on/off control of the GSHP is regulated by the HTF return line temperature, which is related to the outlet temperature T117 of the cylindrical container. As seen in Fig. 9, during the charging period (GSHP on) the inlet temperature T118 presents a higher value than the outlet temperature T117, as corresponds to a positive energy balance of the tank. At the opposite, while the discharging period (GSHP off), the inlet temperature is lower than outlet temperature, the energy balance of the tank being negative. The sequence is repeated on and on till the end of the charging period.

It can be observed that the average temperature of the local charging/discharging modes increases along this period, for example from 51.5ºC to 52.5ºC for probe T117, as the melting of PCM progresses and ends, and the annular liquid phase increase its external temperature. The decreasing branch shows a high slope (only 15 minutes to descent from 53ºC to 49ºC), while at the increasing branch the slope is lower (45 minutes to rise from 49ºC to 53ºC), due to the different result of the energy balance. During the local charging period, both the energy supply (GSHP) and the energy exit (fan-coil) are operating and the net amount of energy entering the tank is the difference between them. Considering the local discharging period, only the energy exit due to the fan-coil is operating, then the absolute energy that leaves the tank is higher than the one of the charging period.

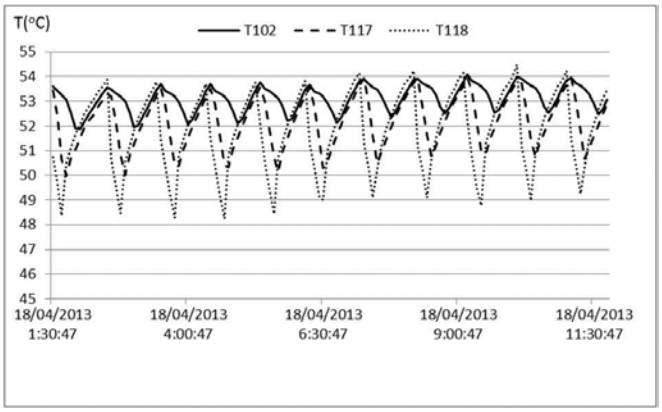


**Figure 9**. Detailed distribution of the HTF temperature vs. time while keeping the set-point temperature (51ºC) of the PCM container.

More complex is the behavior of the HTF measured at the intermediate position, probe T102. As this probe is not placed onto the tube surface but immersed into the HTF flow, its measure is the result of the weighted average between the energy supplied by the HTF and the heat exchange with the PCM tubes, being always more influenced by the HTF flow. For the local charging mode, when the energy balance is positive, the energy exchange is fully dominated by the HTF energy supply, all temperatures increase and, as the heat transfer from the HTF to the PCM takes place, the relative values of temperature follows the sequence

$$T_{118} > T_{102} > T_{117}$$

For the local discharging mode, the energy balance of the storage tank is negative. Temperatures T117 and T118 decrease rapidly but temperature T102 does it slowly. The measured sequence, Fig. 9, is now

$$T_{102} > T_{117} > T_{118}$$

The T102 behavior is now conditioned by heat transfer from the PCM tubes to the HTF, which produces internal gradients of density inside the HTF. The sudden decrease of inlet temperature means the heat is transferred from the external surface of the tubes to the HTF, provoking a local increase of HTF density. This phenomenon around the whole set of tubes lead to a preferential HTF flow through the central part of the tank, with respect to the low density HTF placed at the peripheral part, where probe T102 is placed. This experimental behavior is coherent with theoretical assumptions for the mathematical modelling of heat transfer in similar cases [9]. Then, temperature profile of T102 is delayed with respect T117 and T118 till the charging period starts again.

The same explanation serves for the discharging period of the cylindrical tank, when the energy balance is negative. As long as the HTF evacuates energy from the tank, temperatures T117 and T118 decrease initially while the liquid PCM transfers heat to the HTF. When solidification of PCM begins, a plate shape of temperature profile occurs, keeping the temperature almost constant while the latent heat is transferred. This process means a longer period of energy transfer between the storage system and the facility system (fan-coil), which is one of the advantages of the energy storage approach. After solidification ends, a new period of decreasing temperature appears, the PCM in solid phase. Probe T102 shows the same kind of displacement with respect to the inlet and outlet bulk temperatures as previously stated, due to the peripheral placement of the probe. Finally, at the end of the discharging period, temperatures become closer because of the homogenization of the HTF flow.

**The heat transfer rate between the container and the ambient temperature**

Heat transfer between the storage tank and the surroundings affect the energy balance of the system. At any time, the energy conservation in the storage tank can be expressed as

$$Q_{GSHP} + Q_{PCM} + Q_{EXT} + Q_{FAN} = \frac{\Delta E_{HTF}}{\Delta t} \qquad (2)$$

where $Q_{GSHP}$ is the power supplied by the GSHP; $Q_{PCM}$ is the power absorbed/supplied by the PCM; $Q_{EXT}$ is the heat transfer between the inside of the storage tank and the surroundings; $Q_{FAN}$ s the power extracted by the fan-coil system; and $\Delta E_{HTF}$ is the variation of the energy accumulated by the HTF inside the tank along a period of time $\Delta t$. The aim is to estimate the impact of the heat transfer with the surroundings with respect the accumulation of energy in every functioning period. The energy equation allows the estimation of $Q_{EXT}$ if the rest of the terms of eq. 2 are known.

$Q_{GSHP}$ and $Q_{FAN}$ are determined by its respective energy-meters. $Q_{PCM}$ is estimated by the heat transfer between the HTF and the PCM, once transport properties, flow rates and temperatures are determined. And the $\Delta E_{HTF}$ is computed by means of temperature T102 and the heat capacity of the HTF mass control in the container. Then $Q_{EXT}$ can be obtained. A comprehensive computer program, using Engineering Equation Solver EES software (©F-Chart Software, LLC), has been developed to compute the energy balance in the system. Detailed description of these calculations is outside the scope of this paper, and will be provided in future publications, though some preliminary results were presented in reference [10].

For the purpose of checking experimentally the heat transfer with the surroundings $Q_{EXT}$, heat transfer across the two circular plates at both sides of the tank, and across the cylindrical surface of its length, is evaluated. As the thermal resistance of the insulation is much greater when compared to that of the stainless steel, heat conduction through the stainless steel wall is not considered. Temperature probes T103 and T107 are placed at the respective center of the external surface of the insulated circular plate walls, following Fig. 5. In these surfaces uniform temperature distribution is supposed. Temperature probes T104, T105 and T106 are used to measure the external temperature of the insulation wall at the cylindrical surface. An average of these three temperatures is used as the reference temperature of this surface. As surface temperatures are measured no ambient temperature and external convection is needed.

Concerning the internal convection, only probe T102 is representative of the bulk temperature of the HTF. As stated previously, parallel, counter-current and angular flows could take place in the HTF, then, it is difficult to estimate convection coefficients at different locations of the HTF flow inside the tank. As turbulent flow is supposed, the HTF bulk temperature and the internal surface temperature of the container should be very close, then, we can consider the hypothesis of negligible thermal resistance of the conductive layer with respect to the thermal resistance of the solid conduction (insulation).

Comparison of the experimental estimation of $Q_{EXT}$ under these heat transfer hypothesis with the corresponding value obtained from the energy equation agree quite well, being the average deviation of 2% for the full cycle charge/discharge.

Table 3 shows the results of the evaluation of $Q_{EXT}$ and the estimation of $E_{HTF}$ for the full cycle of the system, as well as for the three partial processes that can de distinguished.

**Table 3**. Estimation of the energy accumulated by the HTF inside the storage tank, $E_{HTF}$, and measured values of the heat transfer between the storage tank and the surroundings $Q_{EXT}$.

| Heat transfer period | $E_{HTF}$ (kJ) | $Q_{EXT}$ (kJ) | $Q_{EXT}/E_{HTF}$ (%) |
|---|---|---|---|
| Total Cycle (average) | 26639 | 10.8 | 0.034 |
| Partial processes (average) | | | |
| Charging period ($<T_{set\ point}$) | 30117 | 10.9 | 0.035 |
| Charging period ($=T_{set\ point}$) | 35753 | 14.8 | 0.041 |
| Discharging period | 22967 | 6.6 | 0.026 |

With respect to the total cycle of the PCM insulated tank, results show that the heat transfer to the surroundings is less than 0.034 % compared to the total amount of energy stored by the HTF, which means that $Q_{EXT}$ is almost negligible in the energy equation.

If we take into consideration the partial processes taking part during the charge/discharge cycle, it can be observed that (i) the average energy content of the HTF inside the tank increases during the charging process before the set point temperature of 50ºC is reached, (ii) energy keeps in the higher value during the saw-tooth period of fixed set point, and (iii) energy decreases to a lower value during the discharging period. The same profile is showed by the heat transfer to the surroundings, increasing as long as the internal temperature (and the energy content) increases, and decreasing when the internal temperature do it, being coherent with the heat transfer dependence on temperature differences. Nevertheless, the ratio $Q_{EXT}/E_{HTF}$ is always very small, less than 0.041%.

## CONCLUSION

A case study of heat transfer study of a low-temperature PCM energy storage system has been presented. The study has

shown data on the characterization of the heat transfer mode of a PCM stored in a horizontal cylindrical shell and tube heat exchanger, being the PCM placed inside the tubes. Some experimental data have been obtained from a bench has been developed to test the heat transfer process.

Some energy transfer processes were studied through the three tests carried on. Concerning the comparison between the radial and the axial heat transfer through the wall of the PCM tube, made of HDPE, experimental data lead to the conclusion that heat transfer along the axial direction is almost negligible compared to the one in the radial direction.

Another issue of interest is the temperature distribution of the HTF along the container, which influences the heat transfer rate to and from the PCM. It has been show that, during periods of positive/negative energy balance and sensible heat exchange with the PCM, the HTF temperatures are dominated by the bulk temperature of HTF, but when melting/solidification processes take place in the PCM, some blockage of peripheral HTF flow can occur due to density gradient.

Finally, in relation with the heat transfer rate between the container and the ambient temperature, experimental data have shown that the heat transfer to the surroundings is negligible compared to the total amount of energy stored by the HTF in the insulated tank, which means that the hypothesis of adiabatic performance is valid.

## AKCNOWLEDGEMENT

We acknowledge support for this research to the firm ENERFUTURE S.L.L., Spain, project on “Integration of low-temperature storage and renewable energy systems in air-conditioning of small scale buildings”, ENERFUTURE-Universidad de Burgos, 2010.

This contribution is part of the Thesis Doctoral of J. M. García-Alonso

## REFERENCES

[1] Dinçer, I., Rosen, M. A., Thermal Energy Storage Systems and Applications, Wiley, London, 2011.

[2] Abhat, A. Low temperature latent heat thermal energy storage: heat storage materials. *Solar Energy*, Vol. 30, No. 4, 1983, pp. 313–32.

[3] Agyenim, F., Hewitt, N., Eames, P., Smyth, M., A review of materials, heat transfer and phase change problems formulation for latent heat thermal energy storage systems (LHTESS), *Renewable and Sustainable Reviews*, Vol. 14, 2010, pp. 615-628.

[4] Ghoneim, A. A., Comparison of theoretical models of phase-change and sensible heat storage for air and water-based solar heating systems, *Solar Energy*, Vol. 42, No. 3, 1989, pp. 209–20.

[5] Hendra, R, Hamdani, Mahlia, T. M. I., Masjuki, H. H., Thermal and melting heat transfer characteristics in a latent heat storage system using mikro, *Applied Thermal Engineering*, Vol. 25, 2005, pp. 1503–15.

[6] Agyenim, F, Eames, P, Smyth, M., Heat transfer enhancement in medium temperature thermal energy storage system using a multitube heat transfer array. *Renewable Energy*, Vol. 35, No. 1, 2010, pp. 198–207.

[7] Gong, Z, Mujumdar A. S., Finite-element analysis of cyclic heat transfer in a shell and tube latent heat energy storage exchanger, *Applied Thermal Engineering*, Vol. 17, No. 4, 1997, pp. 583–91.

[8] Plus Ice©, Phase Change Materials (PCM) Thermal Energy Storage (TES) Design Guide, Phase Change Material Products Ltd, Yaxley, Cambridgeshire, UK, 2011.

[9] Alexiades, V., Solomon, A. D., Mathematical modeling of melting and freezing processes, Hemisphere Publ. Co. Washington, 1993.

[10] García-Alonso, J. M., Aguilar, F., Montero, E., Energy simulation and feasibility of a Ground-Source Heat Pump coupled with a Phase Change Material energy storage system for heat supply, *Renewable Energy & Power Quality Journal*, Vol. 11, 2013, paper 358.